OPTIMIZATION OF GRID CONFIGURATION FOR LEAD-ACID BATTERIES BY INVESTIGATING GRID DEFORMATION *VIA* NUMERICAL MODELING

V. DZENZERSKIY, S. TARASOV, O. SUKHOVA, V. IVANOV, O. DOROSH

Institute of Transport Systems and Technologies of National Academy of Sciences of Ukraine
Pisarzhevsky St. 5, 49005 Dnipro, Ukraine
E-mail: sukhovaya@ukr.net

Received April 28, 2025

Abstract. In this study, numerical methods were employed to investigate the effect of grid configuration, lug position, and wire angles on the stress-deformed state of double rectangular and diagonal grids made of Pb–0.7%Sn–0.08%Ca alloy for VRLA-batteries. The maximum values of stress and displacement were calculated using *SolidWorks* and *ANSYS* programs of finite element analysis. The recommendations were given to optimize design and prevent deformation and distortion of the double grids after solidification, which were confirmed in production conditions.

Key words: VRLA-batteries, double grids, numerical modelling, finite element method, stress-deformed state, optimal grid design.

DOI: https://doi.org/10.59277/RomJPhys.2025.70.911

1. INTRODUCTION

Valve-regulated lead-acid (VRLA) batteries are widely used as a source of electrical energy in vehicles, backup and standby systems for energy storage, telecommunications, household appliances etc. [1–7]. Among many lead-based alloys, ternary Pb–Sn–Ca alloys are used for preparation of VRLA-battery grids because of availability of the raw materials, low cost, ability to age harden at room temperature [9–19], corrosion resistance [20–29], and mechanical properties [30–39]. The grid of lead-acid battery supports mechanically and gives shape to the active material. It also acts as a current carrying collector from the active material.

Grids for VRLA-batteries are manufactured by gravity casting which is presently the principal manufacturing technique employed in the industry [1–3]. In the casting operation, Pb–Sn–Ca alloy ingots are charged to a melting pot, from which the molten alloy flows into casting molds under gravity that form the battery grids of required shape and dimensions upon cooling and solidification. However, deformation and distortion in grids induced by thermal stresses are often observed after solidification [40–46].

As is known, one of the main reasons of casting defects is the creation of an inhomogeneous stress-deformed state throughout the battery grid that determines

the occurrence of stress concentration zones and deformations with significant gradients [47–49]. Therefore, numerical modeling of the displacement and stress distribution through grid wires is an effective, fast, and inexpensive way to optimize the grid configuration [50–61].

The optimization of grid configuration to allow gravity casting with no defects contributes to enhance the overall performance of the VRLA-batteries [62]. This is the reason for the study, the purpose of which is improving the double grid design of VRLA-batteries to investigate and explain the reason of deformation of as-cast grids after solidification and to avoid the re-occurrence of the similar defects in the future.

2. EXPERIMENTAL

In this study, double battery grids were gravity cast of Pb–0.7%Sn–0.08%Ca (in wt.%) alloy in *Wirtz* casting machines of production line for VRLA-batteries of *BM* Company (Austria) at *WESTA* Corp. (City of Dnipro, Ukraine) [63].

To investigate stress and displacement distribution through double grids, finite element modeling was performed using an engineering simulation software (*SolidWorks* and *ANSYS*). All calculations were performed on coarse mesh. Figure 1 shows conventional design of the double middle-lug grid consisting of interconnected vertical and horizontal wires encompassed by a rectangular frame with lugs situated closer to the midpoint of the frames. The places of rigid fixing and loading are indicated by arrows (Fig. 1).

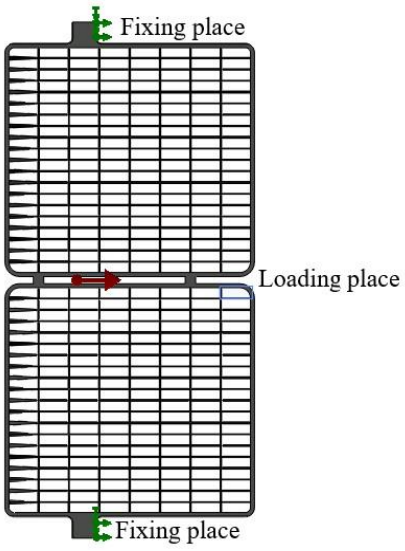

Fig. 1 – Conventional design of double rectangular middle-lug grid.

For the numerical simulation, according to the experiments conducted by the authors [63], the following mechanical characteristics of the Pb–0.7%Sn–0.08%Ca grid alloy were taken: tensile strength of 30 MPa, yield strength of 8 MPa, Young's modulus of 15 GPa, and shear modulus of 49 GPa.

3. RESULTS AND DISCUSSION

SolidWorks software package was used to calculate the stress-deformed state of the double rectangular battery grid of conventional design at each point of its volume by the finite-element method. Using the standard program, *SolidWorks* created a 3D-model of the grid and calculated maximum values of stress and displacement as well as their location (Fig. 2).

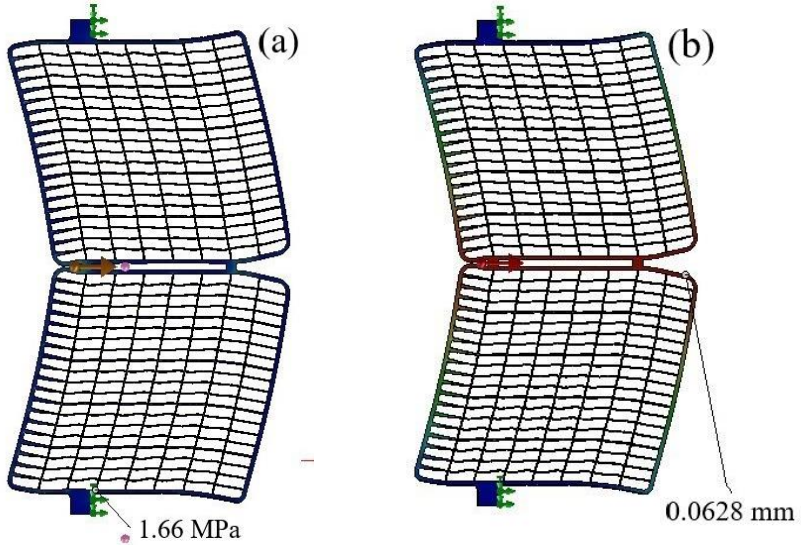

Fig. 2 – Maximum values of stress (a) and displacement (b) of double rectangular middle-lug grid.

The zone of maximal stress is located near the lug, with its value equaling to 1.66 MPa (Fig. 2a). The minimum value of the proportional limit for the Pb–0.7%Sn–0.08%Ca grid alloy exceeds 10 MPa, and therefore maximum value of stress is six times less than that of proportional limit. The maximum value of displacement of 0.06 mm is observed at the junction of single grids into double grid (Fig. 2b).

Figure 3 presents the simulation results of the stress distribution on the lug surface. It clearly indicates that the zone of maximal stress (σ_{max} = 1.66 MPa as mentioned above) is located at the junction of the lug with the third grid wire (Fig. 3a). The highest stress value of 0.099 MPa is found on the lower edge of the

lug, which is 16.8 times less than the maximum value. The difference between the maximum and minimum stress values (1.66 MPa and 0.0021 MPa) indicates the level of nonuniformity of stress distribution through the lug. In all directions across its surface a reduction in the stress values is observed. These values decrease towards the middle of the lug along the outer sides (Fig. 3a). In the middle section of the lug the opposite distribution of stresses is observed (Fig. 3b). The stress values are higher in the central part of the lug than at its edges.

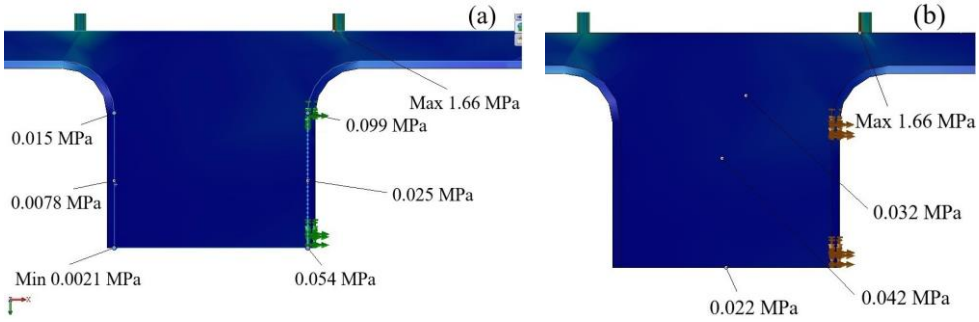

Fig. 3 – Stress distribution through the lug on the outer sides (a) and in the central part (b).

An average level of the stresses taken as a component of compressive stress is determined to be 0.0352 MPa. The values of bending components defined as half the difference of the stress values on the outer sides of the lug vary for its vertical and horizontal sections. The values for vertical sections are 0.042 MPa and 0.008 MPa near the edges and in the center, respectively. The values for horizontal sections amount to 0.0025 MPa, 0.005 MPa, and 0.022 MPa on the upper edge, in the central part, and on the lower edge, correspondingly. Analysis of the computation data shows that the maximum values of bending stresses located near the lug edge exceed those of compressive stresses by 1.2 times. In other locations dominate compressive stresses.

Figure 4 illustrates the stress distributions in the upper and lower jumpers connecting single grids into double grid. It can be calculated from Fig. 4a that the average value of compressive stresses for the upper jumper equals to 0.446 MPa. The values of bending stresses for vertical sections are determined to be 0.198–0.495 MPa near ribs and 0.3 MPa in the middle section. The values of bending stresses for horizontal sections are as follows: 0.295 MPa at the top, 0.058 MPa in the center, and 0.003 MPa at the bottom.

The calculated average value of compressive stresses for the lower jumper is defined to be 0.21 MPa (Fig. 4b). The values of bending stresses for vertical sections amount to 0.1 – 0.12 MPa near ribs and 0.095 MPa in the middle section. For horizontal sections, the values of bending stresses equal to 0.02 MPa at the top, 0.019 MPa in the center, and 0.04 MPa at the bottom.

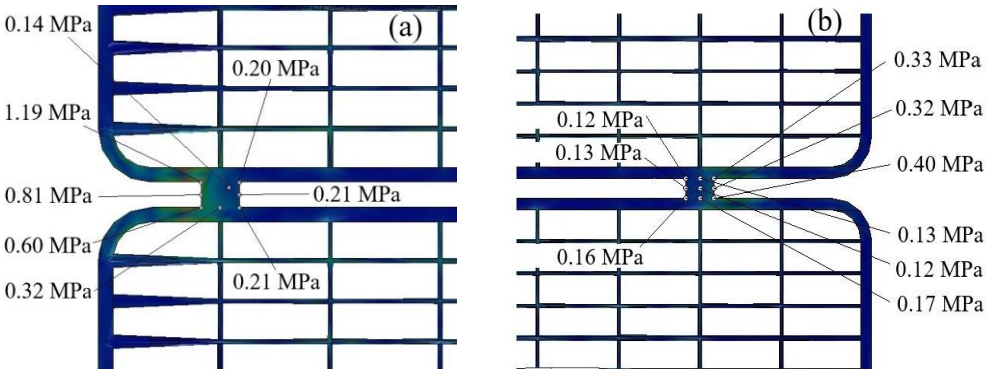

Fig. 4 – Stress state of the upper (a) and lower (b) jumpers connecting single grids into double grid.

Comparative analysis reveals that the values of compressive stresses in the upper jumper exceed those in the lower jumper by 2.4 times. Bending stresses are higher in the upper jumper than in the lower jumper except for the horizontal section at the bottom. The study of stress-deformed state between the lug and the upper jumper shows that the level of stresses in the upper jumper is an order of magnitude higher than that in the lug. The values of stresses in the lower jumper are only several times greater than those in the lug.

Calculated values of displacements in the jumper's zone are shown in Fig. 5.

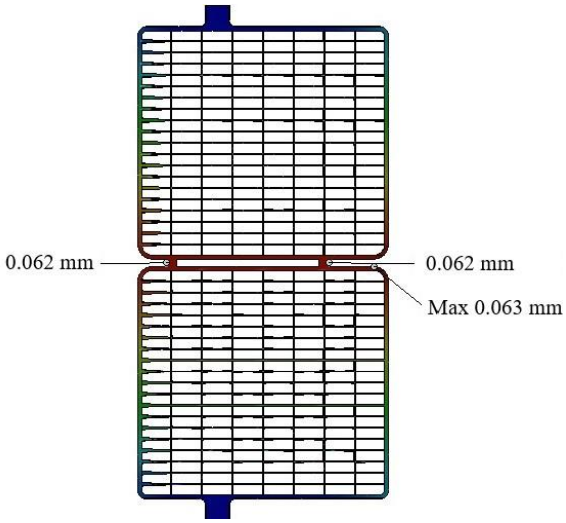

Fig. 5 – Calculated values of displacement in the jumper's zone.

The displacement values for the upper and the lower jumpers are almost the same, with difference in values not exceeding 5–10 mm. Therefore, the vertical forces in the jumpers are suggested to be equal. Furthermore, the displacement

values are only 2.2 % less than the maximum value which amounts to 0.063 mm at the bottom of the double grid (Fig. 5).

Considering obtained simulation results it was concluded that the measures should be taken to strengthen the zone of junction between the single grids. It was proposed to add third jumper to connect single grids into double grid. For a correct analysis of the influence of this change to the design on the stress-deformed state of the grids, *ANSYS* program of finite element method was used. The maximum values of displacement and stress were investigated using two types of double grids with different local geometry such as conventional rectangular grid (Fig. 6a) and diagonal grid (Fig. 6b,c,d). As is known, employing diagonal design which consists of parallel horizontal wires crossed by a series of skewed wires headed toward the lugs instead of rectangular one improves current collecting ability of the grid [62].

The calculated maximum values of displacement and stress of the studied double grid designs are presented in Table 1. The addition of a third jumper at the junction of rectangular middle-lug single grids (Fig. 6a) decreases maximum value of displacement by 1.51 times and that of stress by 1.46 times. These values markedly improve further by directing horizontal wires towards the lug in the double diagonal designs (Fig. 6b,c,d). It is worth mentioning that the reduction in the maximum values of displacement and stress is more pronounced for diagonal grids with the lugs located closer to the midpoint of the frame (Fig. 6c). Positioning the lugs nearer to the midpoint of the grid can also improve the current collecting ability *via* shortening the current path for most part of the grid [62]. The double diagonal middle-lug design with additional third jumper offers the greatest decrease in the maximum values of displacement and stress by 6.43 and 2.84 times, respectively (Fig. 6d), compared to conventional rectangular middle-lug design (Table 1).

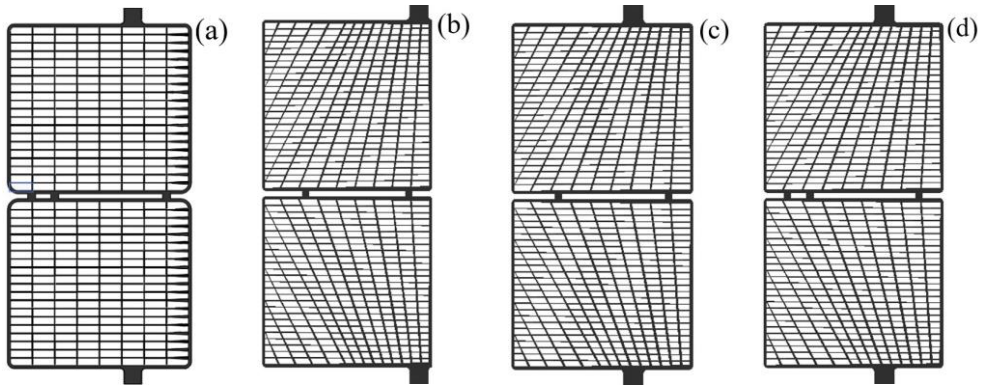

Fig. 6 – Configurations of double rectangular middle-lug grid with additional third jumper at the junction of single grids into double grid (a), double diagonal side-lug grid (b), double diagonal middle-lug grid (c), and double diagonal middle-lug grid with additional third jumper at the junction of single grids into double grid (d).

Table 1

The calculated maximum values of displacement and stress of double grids

Designs of double grids	Displacement, max		Stress, max	
	mm	decrease, times	MPa	decrease, times
Rectangular middle-lug grid	0.0274	–	1.62	–
Rectangular middle-lug grid with additional third jumper at the junction of single grids into double grid	0.0181	1.51	1.11	1.46
Diagonal side-lug grid	0.00584	4.69	0.99	1.64
Diagonal middle-lug grid	0.00565	4.85	0.67	2.42
Diagonal middle-lug grid with additional third jumper at the junction of single grids into double grid	0.00426	6.43	0.57	2.84

4. CONCLUSIONS

Optimal designs of the double rectangular and diagonal grids for VRLA-batteries were chosen in this work. The grids were gravity cast of the Pb–0.7%Sn–0.08%Ca grid alloy in *Wirtz* casting machines of production line for lead-acid batteries. The necessity of changes made to the grid design was estimated based on stress-deformed state analysis *via* numerical modelling.

Calculations carried on the finite element model using *SolidWorks* and *ANSYS* software showed that the maximum value of the stress equaling to 1.66 MPa did not exceed the maximum permissible value of strength of 10 MPa for the Pb– 0.7%Sn–0.08%Ca grid alloy. The maximum values of stress and displacement were observed at the junction of single grids into the double grid. The addition of a third jumper to this zone decreased maximum values markedly, especially for the double grids with diagonal geometry and the lug located closer to the midpoint of the frame. The proposed changes to the design can prevent grid deformation and distortion in the area near the jumpers, which was confirmed in the industrial conditions of VRLA-batteries production at *WESTA* Corp. (City of Dnipro, Ukraine).

REFERENCES

1. S. Guruswamy, *Engineering Properties and Applications of Lead Alloys*, CRC Press, Boca Raton, 2000.
2. D. A. J. Rand, T. Moseley, J. Garche, and C. D. Parker, *Valve-Regulated Lead-Acid Batteries*, Elsevier, Amsterdam, 2004.
3. D. Pavlov, *Lead-Acid Batteries: Science and Technology*, Elsevier, London, 2017.
4. P. Rys, M. Siekierski, M. Knos, and P. Moszczynski, J. Power Technol. **104**, 67–85 (2024).
5. R. D. Prengaman, J. Power Sources **53**, 207–214 (1995).
6. R. D. Prengaman, J. Power Sources **95**, 224–233 (2001).
7. L. Albert, A. Goguelin, and E. Jullian, J. Power Sources **78**, 23–29 (1999).
8. C. S. Lakshmi, J. E. Manders, and D. M. Rice, J. Power Sources **73**, 23–29 (1998).

9. J. P. Hilger and L. Bouirden, J. Alloys Compd. **236**, 224–228 (1996).
10. A. Maitre, G. Bourguignon, J. M. Fiorani, J. Ghanbaja, and J. Steinmetz, Mater. Sci. Eng. A **358**, 233–242 (2003).
11. H. Tsubakino, M. Tagami, and A. Yamamoto, Metall. Mater. Trans. A **27**, 1675–1682 (1996).
12. O. V. Sukhova, East Eur. J. Phys. **2**, 115–121 (2021).
13. D. A. J. Rand, D. P. Boden, C. S. Lakshmi, R. R. Nelson, and R. D. Prengaman, J. Power Sources **107**, 280–300 (2002).
14. L. Bouirden, J. P. Hilger, and J. Hertz, J. Power Sources **33**, 27–59 (1991).
15. J. Hertz, C. Fornasierie, J. P. Hilger, and M. Notin, J. Power Sources **46**, 299–310 (1993).
16. C. Camurri, C. Carrasco, O. Prat, R. Mangalaraja, A. Pagliero, and R. Colàs, Mater. Sci. Technol. **26**, 210–214 (2010).
17. O. V. Sukhova, Phys. Chem. Solid St. **22**(3), 487–493 (2021).
18. A. Maître, G. Bourguignon, G. Medjahdi, E. McRae, and M. H. Mathon, Scr. Mater. **50**, 685–689 (2004).
19. M. Dehmas, A. Maître, J. B. Richir, and P. Archambault, J. Power Sources **159**, 721–727 (2006).
20. R. D. Prengaman, J. Power Sources **67**, 267–278 (1997).
21. E. Gullian, L. Albert, and J. L. Caillerie, J. Power Sources **116**, 185–192 (2003).
22. O. V. Sukhova, V. A. Polonskyy, and K. V. Ustinova, Voprosy Khimii i Khimicheskoi Tekhnologii **3**, 46–52 (2019).
23. K. Sawai, Y. Tsuboi, Y. Okada, M. Shiomi, and S. Osumi, J. Power Sources **179**, 799–807 (2008).
24. O. V. Sukhova, V. A. Polonskyy, and K. V. Ustinova, Voprosy Khimii i Khimicheskoi Tekhnologii **121**(6), 77–83 (2018).
25. G. W. Mao, J. G. Larson, and P. Rao, J. Electrochem. Soc. **120**, 11–17 (1973).
26. O. V. Sukhova, V. A. Polonskyy, and K. V. Ustinova, Metallofiz. Noveishie Tekhnol. **40**(11), 1475–1487 (2018).
27. J. P. Hilger and A. Boulahrouf, Mater. Charact. **24**, 159–167 (1990).
28. O. V. Sukhova and V. A. Polonskyy, East Eur. J. Phys. **3**, 5–10 (2020).
29. Y. Cartigny, J. M. Fiorani, A. Maıtre, and M. Vilasi, Thermochim. Acta **414**, 197–202 (2004).
30. E. Rocca, G. Bourguignon, and J. Steinmetz, J. Power Sources **161**, 666–675 (2006).
31. H. Li, W. X. Guo, H. Y. Chen, D. E. Finlow, H. W. Zhou, C. L. Dou, G. M. Xiao, S. G. Peng, W. W. Wei, and H. Wang, J. Power Sources **191**, 111–118 (2009).
32. F. Rossi, M. Lambertin, L. Delfaut-Durut, A. Maitre, and M. Vilasi, J. Power Sources **185**, 1465–1470 (2008).
33. O. V. Sukhova, V. A. Polonskyy, and K. V. Ustinova, Mater. Sci. **55**(2), 291–298 (2019).
34. M. T. Wall, Y. Ren, T. Hesterberg, T. Ellis, and M. L. Young, J. Energy Storage **55**, 6–13 (2022).
35. B. Yang, C. Xianyu, Y. Shaoqiang, L. Wei, D. Changsong, and Y. Geping, J. Energy Storage **25**, 1–9 (2019).
36. Y. B. Zhou, C. X. Yang, W. F. Zhou, and H. T. Liu, J. Alloys Compd. **365**, 108–111 (2004).
37. D. Slavkov, B. S. Haran, B. N. Popov, and F. Fleming, J. Power Sources **112**, 199–208 (2002).
38. V. O. Dzenzerskiy, S. V. Tarasov, O. V. Sukhova, and V. A. Ivanov, Rom. J. Phys. **69**, 605 (2024).
39. V. O. Dzenzerskiy, S. V. Tarasov, O. V. Sukhova, and V. A. Ivanov, East Eur. J. Phys. **4**, 182–188 (2023).
40. I. Spiridonova, O. Sukhova, and O. Vashchenko, Metallofiz. Noveishie Tekhnol. **21**, 122–125 (1999).
41. B. Trembach, Y. Silchenko, O. Balenko, D. Hlachev, K. Kulahin, H. Heiko, O. Bellorin-Herrera, S. Khabosha, O. Zakovorotnyi, and I. Trembach, Int. J. Adv. Manuf. Technol. **134**(1–2), 309–335 (2024).
42. O. V. Sukhova, Probl. At. Sci. Technol. **128**(4), 77–83 (2020).
43. I. M. Spiridonova, E. V. Sukhovaya, S. B. Pilyaeva, and O. G. Bezrukavaya, Metallurgicheskaya i Gornorudnaya Promyshlennost **3**, 58–61 (2002).
44. V. G. Efremenko, Yu. G. Chabak, V. I. Fedun, K. Shimizu, T. V. Pastukhova, I. Petryshynets, A. M. Zusin, E. V. Kudinova, and B. V. Efremenko, Vacuum **185**, 110031 (2021).

45. M. Krbata, M. Kohutiar, J. Escherova, P. Klučiar, Z. Studeny, B. Trembach, N. Beronská, A. Breznická, and Ľ. Timárová, Appl. Mech. **6**(1), 16 (2025).
46. O. V. Sukhova and K. V. Ustinova, Funct. Mater. **26**(3), 495–506 (2019).
47. V. G. Efremenko, A. G. Lekatou, Yu. G. Chabak, B. V. Efremenko, I. Petryshynets, V. I. Zurnadzhy, S. Emmanouilidou, and M. Vojtko, Mater. Today Commun. **35**, 105936 (2023).
48. I. M. Spyrydonova, O. V. Sukhova, and G. V. Zinkovskij, Metallurgical and Mining Industry **4**(4), 2–5 (2012).
49. Yu. G. Chabak, K. Shimizu, V. G. Efremenko, M. A. Golinskyi, K. Kusumoto, V. I. Zurnadzhy, and A. V. Efremenko, Int. J. Miner. Metall. Mater. **22**, 78–87 (2022).
50. D. Redchyts, S. Dovgiy, U. Tuchyna, and S. Moiseienko, *Using Mathematical Simulation to Improve the Selective Laser Melting Process for 3D Printing*, S. Dovgiy, E. Siemens, L. Globa, O. Kopiika, and O. Stryzhak (eds.), in *Applied Innovations in Information and Communication Technology*, Springer, Cham, 2025, pp. 672–694.
51. J. Grydzhuk, I. Chudyk, O. Slabyi, Yu. Mosora, M. Kovbaniuk, and M. Krynke, Prod. Eng. Arch. **28**, 375–380 (2022).
52. D. Redchyts, A. Ballesteros-Coll, U. Fernandez-Gamiz, U. Tuchyna, O. Polevoy, S. Moiseienko, and V. Zaika, AIAA J. **62**(7), 2548–2561 (2024).
53. B. O. Trembach, Y. A. Silchenko, M. G. Sukov, N. B. Ratska, Z. A. Duriagina, I. V. Krasnoshapka, O. B. Kabatskyi, and O. M Rebrova, Mater. Sci. **59**(6), 733–740 (2024).
54. S. Moiseienko, U. Tuchyna, D. Redchyts, V. Zaika, and I. Vygodner, *Comparative Analysis of Numerical Methods for Solving Linear Equation Systems for Poisson's equation*, H. Altenbach, A. H.-D. Cheng, X.-W. Gao, A. Kostikov, W. Kryllowicz, P. Lampart, V. Popov, A. Rusanov, and S. Syngellakis (eds.), in *Advances in Mechanical and Power Engineering*, Springer, Cham, 2021, pp. 169–177.
55. M. Voncina, J. Medved, G. Segel, and T. Balasko, Mater. Technol. **59**, 143–149 (2025).
56. D. O. Redchyts and S. V. Moiseienko, Space Sci. Technol. **27**(1), 85–96 (2021).
57. P. A Belonozhko, M. M. Zhechev, and S. V. Tarasov, Sov. Appl. Mech. **7**, 683–688 (1986).
58. D. Redchyts, U. Fernandez-Gamiz, O. Polevoy, S. Moiseienko, and K. Portal-Porras, Energy Sources A: Recovery Util. Environ. **45**(4), 9993–10009 (2023).
59. V. L. Kulakov, Yu. M. Tarnopol'skii, A. K. Arnautov, and J. Rytter, Mech. Compos. Mater. **40**, 145–160 (2004).
60. J. S. Musayev, T. O. Chigambaev, Y. B. Kaliyev, B. T. Kopenov, M. Zh. Turkebayev, M. A. Nartov, and A. Zhauyt, Metalurgija **59**, 340–342 (2020).
61. V. O. Dzenzerskiy, S. V. Tarasov, D. O. Redchyts, V. A. Ivanov, and O. V. Sukhova, J. Nano-Electron. Phys. **16**(1), 01003 (2024).
62. A. Alagheband, M. Azimi, H. Hashemi, M. Kalani, and D. Nakhaie, J. Energy Storage **12**, 202–214 (2017).
63. V. Dzenzerskiy, S. Tarasov, O. Sukhova, and V. Ivanov, Rom. J. Phys. **69**(7–8), 907 (2024).